ACS Sustainable Chemistry & Engineering

Research Article

pubs.acs.org/journal/ascecg

Silver Nanoparticle-Induced Growth of Nanowire-Covered Porous MnO_2 Spheres with Superior Supercapacitance

Yuming Dai,[†,‡,§] Shaochun Tang,[†,§] Sascha Vongehr,[†] and Xiangkang Meng*[,†]

[†]Institute of Materials Engineering, National Laboratory of Solid State Microstructures, College of Engineering and Applied Sciences, Nanjing University, Jiangsu, P.R. China

[‡]School of Materials Engineering, Nanjing Institute of Technology, Jiangsu, P.R. China

Supporting Information

ABSTRACT: We report a facile, low-cost, ultrasound-assisted synthesis of nanowire-covered porous MnO_2 spheres with superior supercapacitance at high charging rates with long-term durability. The use of catalytic silver nanoparticles is crucial to the growth mechanism in the initial stage, and the resulting silver oxides later grow the nanowires in such a way that they always terminate the wires, thus automatically covering the structures and increasing conductivity. The optimal Ag_2O-MnO_2 structures have a specific capacitance of 536.4 F/g at 5 mV/s. At a high scan rate of 100 mV/s, only 200 F/g remain for the reported carbon nanotube/MnO_2 material with an excellent capacitance at low scan rate (1230 F/g, 1 mV/s), while the Ag_2O-MnO_2 reported here still has 417.2 F/g. The material reaches a stable region of 91.3% capacitance retention over 10000 charge/discharge cycles at 5 A/g.

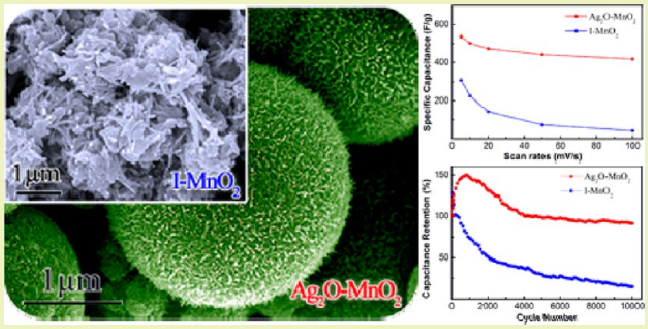

KEYWORDS: *Manganese oxide, Supercapacitors, Hierarchical structures, Rapid charging, Long-term stability*

INTRODUCTION

One difficulty with supercapacitors is their performance in rapid charge/discharge applications.[1] High capacitance and long-term stability at high charging rates need electrode materials with a high surface area, stable microstructure, and good electrical conductivity.[2] Because of their pseudocapacitance,[3−6] transition metal oxides have larger specific capacitance (SC) than carbon materials or conducting polymers.[7,8] RuO_2 performs best among the oxides, but high cost limits its commercial applications.[9,10] MnO_2 is one of the most promising alternatives because of its high theoretical SC (1370 F/g), low cost, and environmental compatibility.[11−14] However, in part due to its poor electrical conductivity, the actual SC during rapid charge/discharging is usually low.[1]

The electrical conductivity of electrode materials can be improved by combining them with conductive materials including carbon materials,[15−18] conductive oxides like SnO_2[19] and Zn_2SnO_4,[20] and metals such as gold film.[21] However, a combination of conductive oxides with MnO_2 usually needs multi-step coating processes. We will show that our Ag nanoparticle-induced growth process results in a hierarchical nano/microstructure being covered with automatically formed conductive Ag_2O, which is due to a novel growth process.

Regular shapes and especially one-dimensional nanostructures of transition metal oxides, such as nano wires, rods, and tubes, perform better electrochemically than those with irregular shapes.[22,23] Hierarchical architectures that involve such nanostructures are more likely to have stable SC because their microsized substrates fix the nanoporous structure.[24−27] Inspired by this, great progress in developing MnO_2-based supercapacitive materials has been made via hierarchical nano/microcomposites. However, the SC is still usually much lower with rapid charging and becoming unstable over time, especially with rapid charge/discharge cycles. Recently, electrochemical growth of nanostructured MnO_2 on porous nanogold film[21] and on sponge-dipped carbon nanotubes[15] approached the theoretical SC of MnO_2 (1370 F/g)[28] but only at low charge/discharge rates (e.g., 1 mV/s); the SC decreases to ~300 F/g at 50 mV/s.[15] $Zn_2SnO_4-MnO_2$ microfiber hybrid composites show a SC of 621.6 F/g at 2 mV/s; but only 370 F/g remain at 100 mV/s.[20] The costs associated with these materials are high. In addition, long-term stability needs to be improved with MnO_2-based devices.

In this work, we report a facile and low-cost ultrasound-assisted synthesis of nanowire-covered spherical MnO_2 structures with high SC with rapid charging and discharging, while long-term durability is also promising. The use of catalytic silver nanoparticles (NPs) is crucial to adjust the growth rates of MnO_2 in the initial and final stages. The electrical conductivity of the material is improved due to the silver oxides being crucially involved in the growth of the nanowires

Received: October 4, 2013
Revised: December 13, 2013
Published: January 5, 2014

in such a way that they are always at the wire tips. The SC is optimized via a systematic variation of concentrations and reaction times, leading to a dense yet short "British-lawn" or rather "AstroTurf-like" nanowire cover over the spheres. The growth mechanism is suggested on the basis of composition and microstructure analysis as well as systematic control experiments. The resulting Ag_2O−MnO_2 structures have a SC of 536.4 F/g at 5 mV/s, which is almost twice the value attainable with pure MnO_2 structures.[4] This is not the highest SC reported, as discussed above; however, the new material still has 78% of the static SC during rapid charge/discharge cycles. At a high scan rate of 100 mV/s, only 200 F/g remain for the carbon nanotube−MnO_2 material with the excellent reported SC (1230 F/g)[15] at a low scan rate of 1 mV/s, while the Ag_2O−MnO_2 reported here still has 417.2 F/g.

EXPERIMENTAL SECTION

Synthesis of Ag Nanoparticles. For solution A, 5 mmol (0.85 g) $AgNO_3$ was dissolved in 10 mL deionized water. For solution B, 2 mmol (0.22 g) NaH_2PO_2 was dissolved in 40 mL deionized water. Solution A was added to solution B at 20 drops/min under a violent stir. The mixture was ultrasonicated for 1 h in a thermostatic water bath at 50 °C. The precipitates were collected by centrifugation and repeatedly washed with deionized water.

Synthesis of Ag_2O−MnO_2 Hierarchical Structures. Four mmol (0.68 g) $MnSO_4$ and 4 mmol (0.92 g) $(NH_4)_2S_2O_8$ were dissolved in 40 mL deionized water. Eight milligrams of preprepared dried Ag nanoparticles were added. The mixed solution was ultrasonic irradiated for 1 h in a thermostatic water bath at 50 °C. The precipitates were collected, washed, and finally dried in a vacuum oven at 50 °C for 12 h.

Characterizations. The products were characterized with X-ray diffraction (XRD, Ultima-IV, Rigaku) using Cu Kα radiation at a scan rate of 10°/min, X-ray photoelectron spectroscopy (XPS, ESCA2000, Thermo) with a CLAM4 hemispherical analyzer, field-emission scanning electron microscopy (SEM, S-4800, Hitachi) at 10 kV, and transmission electron microscopy (TEM, JEM-2100, JEOL) at 200 kV. Energy dispersed X-ray spectroscopy (EDS) was performed on the same scanning electron microscope. The specific surface areas were determined by Brunauer−Emmett−Teller (BET) methods using a surface area analyzer (Tristar-3000, Gold-APP).

Electrochemical Measurements. Cyclic voltammetry (CV) was performed on a workstation (PARSTAT 2273, Ametek) using a three-electrode mode in a 1 M Na_2SO_4 aqueous solution at room temperature. The working electrodes were prepared by mixing and grinding the active materials (70 wt %), acetylene black (20 wt %), and 10 wt % polytetrafluoroethylene for about 20 min with a small amount of ethanol. Then, the mixture was coated onto nickel foam (1 cm^2) to form the electrode layer by drying at 120 °C for 10 h. After that, the electrode layer was compressed with 10 MPa. The reference and counter electrodes were Ag/AgCl and platinum foil, respectively. The electrochemical performances of MnO_2-based electrodes were tested using CV between 0 and 1 V at scan rates of 5, 10, 20, 30, 50, and 100 mV/s. Specific capacitance (SC) of MnO_2 was calculated using the following formula

$$SC = \int i dV / vm\Delta V$$

where $\int i dV$ is the integral area under the CV curve calculated by the software, v is the scan rate, m is mass of the active material, and ΔV is the operating potential range. Galvanostatic measurements were on a workstation (CHI660D, Chenhua) using the same electrolytic cell as the CV tests at a charge/discharge current density of 5 A/g and a potential window of 0 to 1 V. Capacitance retention was tested on a battery analyzer (C5 V100 mA, BettaTeQ). The anode is the same as the above-described working electrode, and the cathode is blank nickel foam. They were assembled by using polyethylene (PE) fibrous paper as the separator and 1 M Na_2SO_4 aqueous solution as the electrolyte. The current density and potential windows are the same as those in the galvanostatic measurements. The capacitance retention of any cycle equals its discharge time divided by the discharge time of the first cycle.

RESULTS AND DISCUSSION

Microscopic and Structural Analysis. A low-magnification SEM image (Figure 1a) shows that the optimized product, which is obtained after a reaction time of 1 h, consists of isolated particles having uniform spherical morphology with a diameter of 2.2 ± 0.6 μm. A high-magnification image (Figure 1b) reveals that their surfaces are uniformly covered in nanowires. The nanowires have a diameter of 15 ± 5 nm (inset Figure 1b) and stand almost upright on the surface rather than lying on top of it. The free ends of the wires all terminate in a white dot.

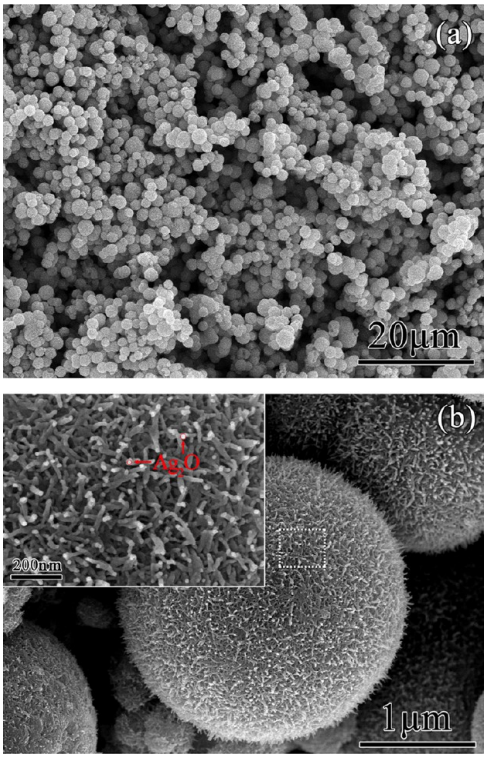

Figure 1. (a) Low and (b) high magnification SEM images of Ag_2O−MnO_2 structures; the inset further magnifies the marked rectangle.

TEM observation (Figure 2a) shows the cross-section of the nanowire cover more clearly. A high-resolution TEM (HRTEM) image (Figure 2b) recorded from a free end of a nanowire gives interplanar spacings of 0.27 and 0.24 nm, consistent with the distances of the (111) planes of Ag_2O (as also confirmed by X-ray photoelectron spectroscopy (XPS) analysis—see below) and (211) planes of MnO_2. Fast Fourier transform (FFT) patterns further confirm that the crystal planes in the selected areas correspond to those ofAg_2O (111) and MnO_2 (211). The Ag_2O resides on the end of the MnO_2 nanowires (inset Figure 1b); thus the white dots in the SEM images are Ag_2O.

In the absence of silver, the reaction is much slower, and irregular MnO_2 (I-MnO_2) nanostructures were synthesized only after 4 h. A low-magnification SEM image (Figure S1a, Supporting Information) shows that the products are loose-packed rather irregular shapes. Further magnification (inset) reveals that the surface consists of plates and not wires.

dx.doi.org/10.1021/sc400403q | ACS Sustainable Chem. Eng. 2014, 2, 692−698

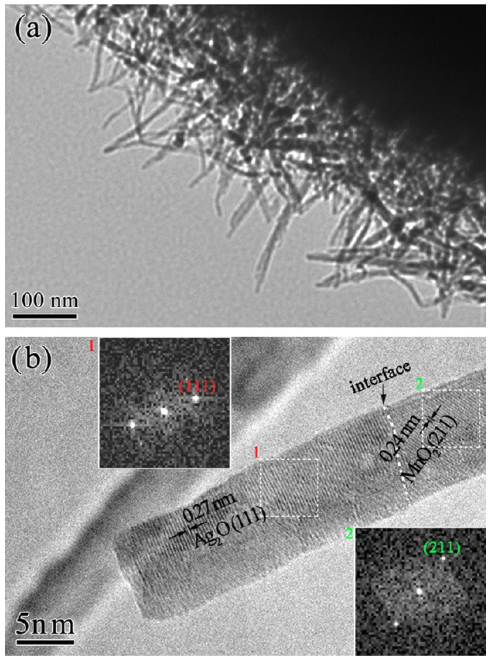

Figure 2. (a) TEM and (b) HRTEM images of the product shown in Figure 1.

Figure 3a shows X-ray diffraction (XRD) patterns of the Ag_2O–MnO_2 and I-MnO_2 products. All the diffraction peaks correspond to the crystal planes of MnO_2 (JCPDS no. 44-0141). A higher diffraction intensity and the presence of diffraction peaks corresponding to (310), (211), (301), (411), and (521) planes indicate that the Ag_2O–MnO_2 product has a higher crystallinity than I-MnO_2. Peaks for Ag and Ag_2O cannot be found due to their low content in the resulting Ag_2O–MnO_2. XPS surveys (Figure 3b) show the Mn $2p_{3/2}$ (641.7 eV) peak attributed to MnO_2. The Ag $3d_{5/2}$ (367.6 eV) and Ag $3p_{3/2}$ (573.4 eV) peaks correspond to Ag_2O and Ag, respectively. The spectra of O 1*s* (Figure 3c) of the Ag_2O–MnO_2 sample showed that it consists of an O 1*s* (MnO_2) peak (529.6 eV) and O 1*s* (Ag_2O) peak (530.9 eV). The area ratio of O 1*s* (Ag_2O):O 1*s* (MnO_2) is about 1:15. The result further proves that the sample consists of Ag_2O and MnO_2. The total Ag atomic percentage is 2.11%. This is higher than the energy dispersed X-ray spectroscopy (EDS) result of 0.97% (Figure S2, Supporting Information). XPS analysis collects information of several nanometers depth away from the outer surface of samples, while EDS reaches hundreds of nanometers inside. Thus, the results confirm the presence of Ag_2O on the surface.

Growth Mechanism of Ag_2O–MnO_2 Hierarchical Structures. The growth mechanism is suggested as follows (Figure 4). The Ag NPs (Figure S1c, Supporting Information) dissolve slowly in the presence of $(NH_4)_2S_2O_8$ into 1.85 mM Ag^+ ions. They are completely dissolved only after about 10 min even in the absence of $MnSO_4$ (where the dissolution can be clearly seen) and must be expected to dissolve even slower in the presence of $MnSO_4$. Control experiments using $AgNO_3$ solutions with different concentrations around this value (namely, 0.1, 1.0, and 10 mM) instead of Ag NPs did not obtain spherical MnO_2 that are as densely covered with nanowires (Figure S3, Supporting Information). The growth of MnO_2 particles will not be noticeable for 30 min without any Ag. Thus, Ag is necessary from the start, but the release of Ag^+ ions must be slow for the formation of the desired structures.

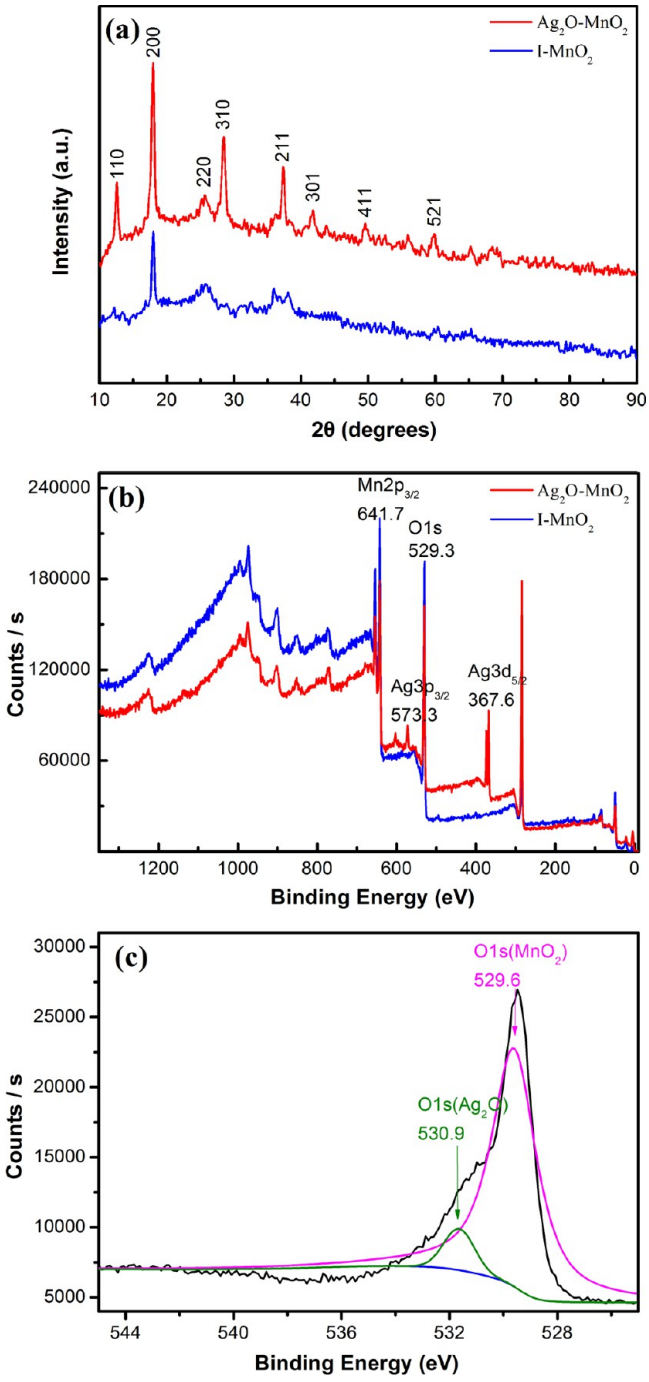

Figure 3. (a) XRD patterns and (b) XPS surveys of the Ag_2O–MnO_2 and I-MnO_2. (c) XPS spectra of O 1s of Ag_2O–MnO_2.

Addition of 1.85 mM $AgNO_3$ via slow dripping (over 5, 10, and 20 min for Figure S4a–c, Supporting Information, respectively) also does not lead to the desired structures. We have not been able to replace the Ag nanoparticles with any time-dependent addition of Ag^+ ions. Therefore, the presence of catalytic Ag nanoparticles is crucial directly; their role is not exhausted in simply providing a slow addition of ions.

The dissolution of Ag NPs in $(NH_4)_2S_2O_8$ releases oxygen. In the presence of Ag^+ and Ag_2O on the Ag NPs acting catalytically, Mn^{2+} ions are oxidized by the released oxygen and $(NH_4)_2S_2O_8$. Because of the subsequently high concentration of MnO_2, a rapid nucleation ensues. The MnO_2 nuclei combine

dx.doi.org/10.1021/sc400403q | ACS Sustainable Chem. Eng. 2014, 2, 692–698

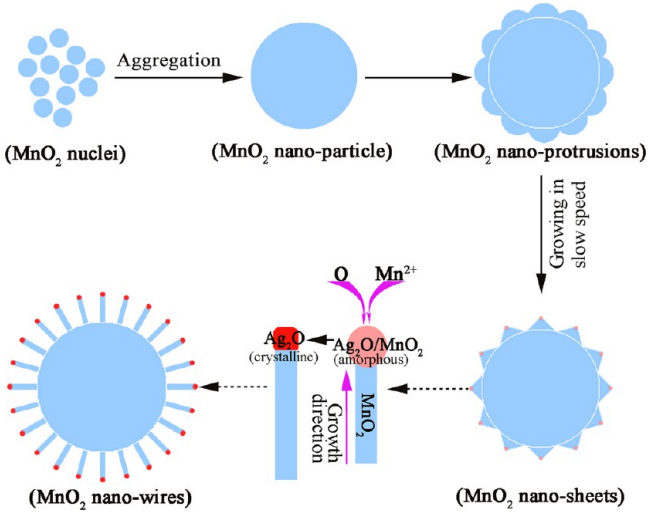

Figure 4. Schematic illustration of the growth process of Ag_2O–MnO_2.

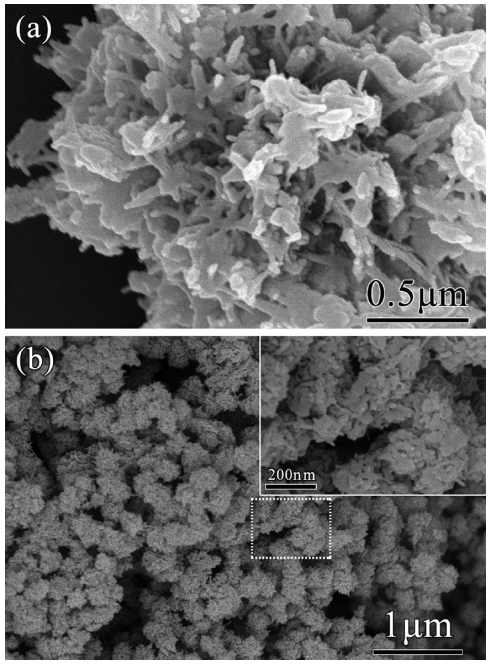

Figure 6. SEM images of Ag_2O–MnO_2 products obtained (a) in the absence of any agitation and (b) stirring instead of ultrasound. Other reaction conditions are the same as those for the optimal Ag_2O–MnO_2 structures. Insets are further magnifications of the marked rectangle.

to form small crystallites. Because of the minimization of surface energy, these crystallites aggregate into spherical shapes (Figure 5a). These steps are not rapid without Ag being present, and the absence of Ag leads to nonspherical aggregates of plate-like NPs (I-MnO_2; Figure S1a, Supporting Information). Ultrasound is also crucial for the formation of the desired product. No agitation at all or stirring resulted in large aggregates with rough flaky surfaces (Figure 6). This crucial influence on the growth mechanism has been seen previously in the synthesis of spherical porous palladium nanostructures.[29] Besides avoiding and breaking up of larger aggregates,

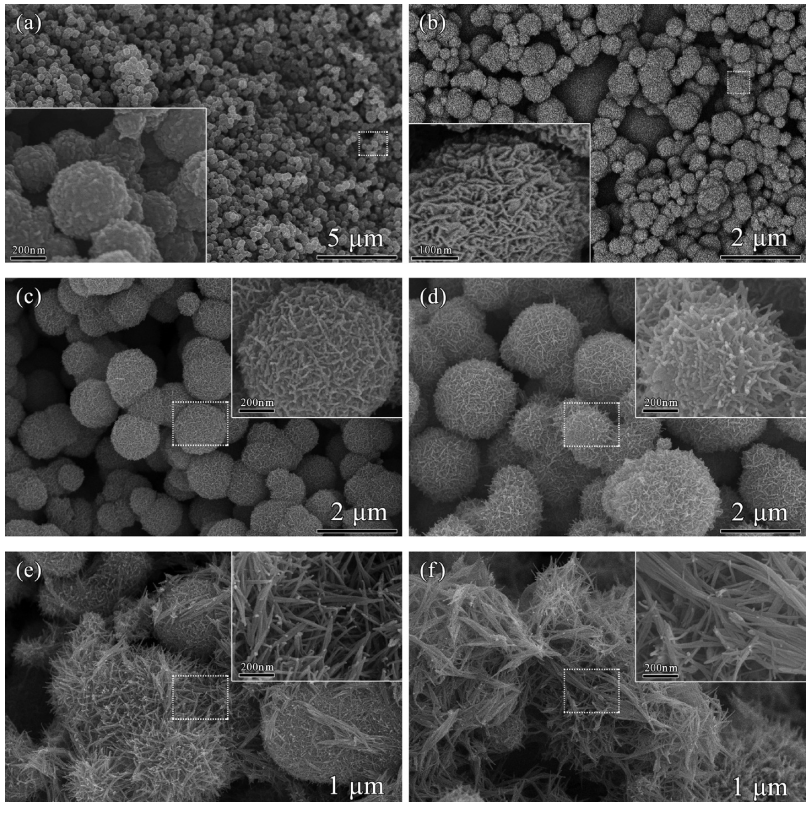

Figure 5. SEM images of the products obtained after different reaction times but otherwise under the same conditions as those for the synthesis of the optimal Ag_2O–MnO_2: (a) 1 min, (b) 5 min, (c) 30 min, (d) 120 min, (e) 240 min, and (f) 480 min. Insets are further magnifications of the marked rectangle.

dx.doi.org/10.1021/sc400403q | ACS Sustainable Chem. Eng. 2014, 2, 692–698

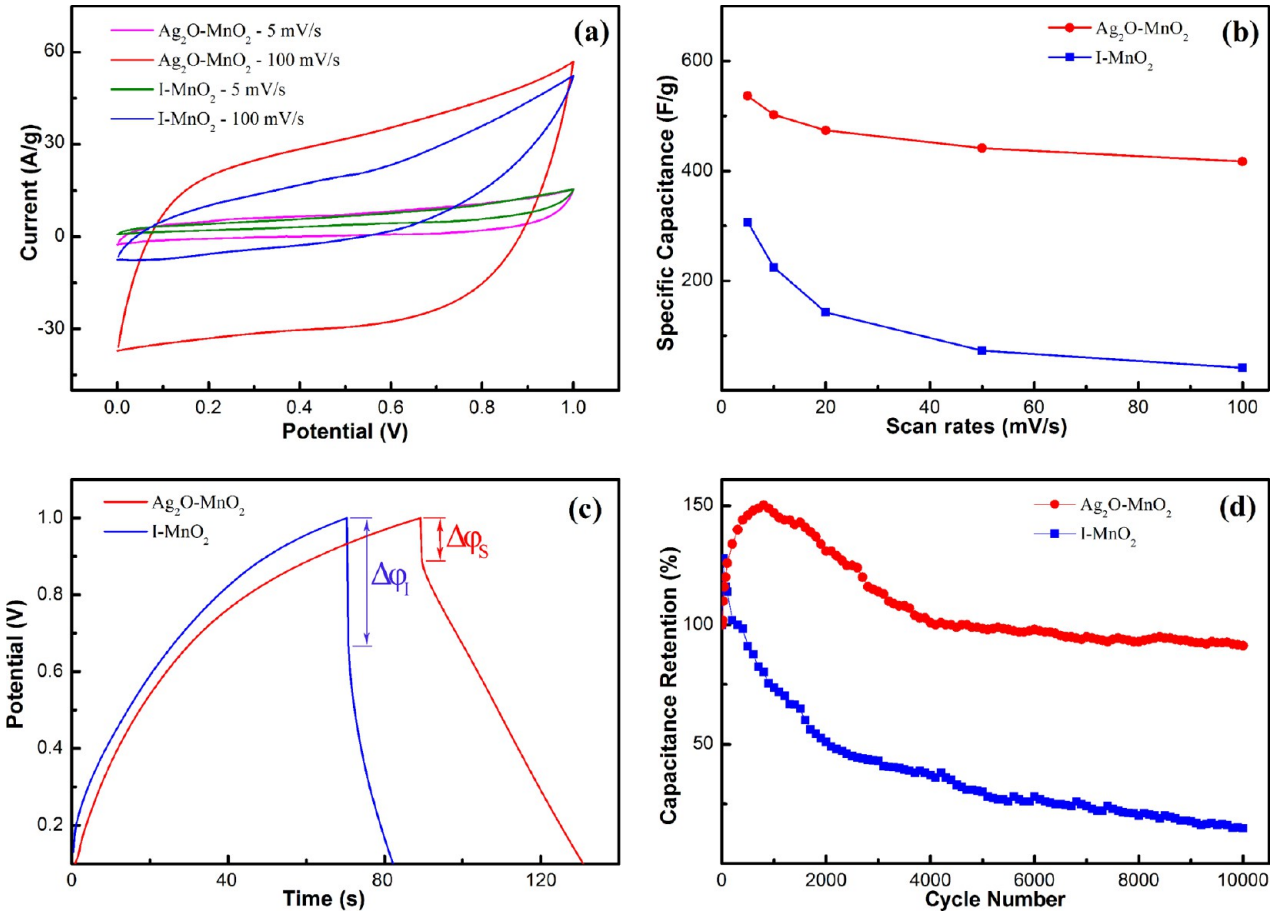

Figure 7. Electrochemical performance of the Ag_2O−MnO_2 and I-MnO_2 electrodes measured in 1 M Na_2SO_4 solution. (a) CV curves at scan rates of 5 and 100 mV/s. (b) SC versus scan rates. (c) Galvanostatic charge/discharge curves at a current density of 5 A/g. (d) Capacitance retention at 5 A/g over 10,000 cycles.

ultrasound improves the transport of crystallites in the solution, leading to denser spheres rather than allowing the growth of flakes first. With a decrease in Mn^{2+} concentration, nucleation of crystallites and growth of new spheres stop, and the remnant Mn^{2+} adds to the already present spheres. An anisotropic growth builds nanosheets on the spheres' surfaces (Figure 5b, c). The ongoing dissolution of the Ag NPs increases the Ag^+ ion concentration; thus Ag oxide starts to build up on the surface of the growing nanostructures. Ag_2O does not join into the MnO_2 crystal lattice, but amorphous Ag_2O−MnO_2 puddles gather and stay on the outside of the spheres. These now orientate the growth of MnO_2 away from the sphere surface as follows. Just as during nucleation, Ag_2O catalyzes oxidation of Mn^{2+}, but now the Mn^{2+} concentration is low. Instead of nucleation and growth of MnO_2 particles being triggered, Mn oxide diffuses through the amorphous Ag_2O−MnO_2 and deposits onto the pure MnO_2 crystal of the microsphere below. Therefore, the amorphous Ag_2O−MnO_2 lifts itself from the MnO_2 surface, and nanowires form below. This is similar to the solution−liquid−solid growth scenario[30] and the vapor−liquid−solid growth of Mn-terminated InAs nanowires.[31] When no more Mn^{2+} is available, the MnO_2 concentration in the amorphous Ag_2O−MnO_2 goes to zero as the last remaining MnO_2 inside of it attaches to the MnO_2 nanowire. Being now pure Ag_2O, the crystallization of the Ag oxide is the last step, leading to the nanowire tips of pure Ag_2O shown in Figure 2b. The analysis of samples taken at different times during the reaction verifies this picture because the Ag_2O is always at the end of the nanowires, regardless of whether the product has been removed after 1 h or at later times, say after 2, 4, or 8 h (Figure 5d−f, respectively). The samples taken at different times show that the nanowires were still growing at those times; yet the Ag_2O always terminates the wires because it crystallized after the product had been removed from the Mn^{2+}-rich reaction solution.

Electrochemical Studies. Figure 7a shows cyclic voltammetry (CV) curves of the Ag_2O−MnO_2 and the I-MnO_2 at scan rates of 5 and 100 mV/s. The rectangularity of the curves implies that the capacitances are mainly associated with Faradic pseudocapacitance.[32] The Ag_2O−MnO_2 curves are more symmetric than those for I-MnO_2. Figure 7b shows the corresponding SC at various scan rates from 5 to 100 mV/s. The SC of the Ag_2O−MnO_2 is 536.4 F/g at a scan rate of 5 mV/s, which is nearly twice that of the I-MnO_2 (306.9 F/g) and the extremely high reported value for pure MnO_2 supercapacitive materials (309 F/g, 5 mV/s).[4] This is partly attributed to the higher specific surface area of Ag_2O−MnO_2 (92 m^2/g) compared to the I-MnO_2 (36 m^2/g).

The performance of Ag_2O−MnO_2 becomes interesting at high scan rates like 100 mV/s, where its SC is 12 times that of MnO_2 nanowires (Figure S5a, Supporting Information) with a similar diameter as the nanowires on top of the spheres (Figure 1b, inset). The Ag_2O−MnO_2 samples obtained with the reaction times of 30, 60, 120, 240, and 480 min exhibit SC

dx.doi.org/10.1021/sc400403q | ACS Sustainable Chem. Eng. 2014, 2, 692−698

values of 381.7, 417.2, 352.6, 295.1, and 217.2 F/g, respectively (Figure S6, Supporting Information). Thus, the high SC of the optimal Ag_2O-MnO_2 is due to a dense yet short "British-lawn"-like coverage of the spheres by nanowires. At 100 mV/s, the SC of I-MnO_2 is 41.6 F/g, only 10% of the low scan rate value. Such a decrease at high scan rates is quite usual. For example, Zn_2SnO_4-covered MnO_2 (621.6 F/g at 5 mV/s) and MnO_2 on sponge-dipped carbon nanotubes (1230 F/g at 1 mV/s) have higher SC values than all our products at low scan rates. However, at 100 mV/s, only 370 F/g remains for Zn_2SnO_4-covered MnO_2[20] and only 200 F/g for sponge-dipped carbon nanotubes.[15] Our Ag_2O-MnO_2 still has a SC of 417.2 F/g even at 100 mV/s (78% of the low scan rate SC); the value is to our knowledge the highest SC reported for Mn oxide-based electrode materials at high scan rates, making it a very promising material for high charge/discharge applications.

The presence of Ag_2O benefits the SC at high scan rates because it facilities electron transport between MnO_2 and the external environment. The potential jumps $\Delta\varphi_I$ for I-MnO_2 (Figure 7c), MnO_2 nanowires (Figure S5b, Supporting Information), and Ag_2O-MnO_2 (Figure 7c) are 0.329, 0.219, and 0.114 V, respectively, showing the latter to have the highest conductivity. At a current density of 5 A/g, the discharge time of Ag_2O-MnO_2 (47.6 s) is three times that of I-MnO_2 (16.0 s), meaning that the SC of Ag_2O-MnO_2 is three times that of I-MnO_2, consistent with the CV tests.

Figure 7d shows the capacitance retention of Ag_2O-MnO_2 and I-MnO_2 at a current density of 5 A/g. In the initial stage, the values of the two samples both increase, and the I-MnO_2 reaches the maximum value (128.1%) only at 25th cycle. However, the capacitance retention of the Ag_2O-MnO_2 is 150.2% after about 800 cycles. This interesting phenomenon is due to self-activation; it could be attributed to the active process of the electrode.[33] The hierarchical superstructures of the Ag_2O-MnO_2 bring much a stronger effect of self-activation. After the initial increase, the capacitance of I-MnO_2 decreases monotonously. The Ag_2O-MnO_2 returns to about 100% of the initial SC at around 4000 cycles, after which it stays surprisingly stable, decreasing slowly to 91.3% at the completion of 10,000 cycles. Given the initial 4000 cycles, clearly the material cannot be said to be especially stable; however, a surprisingly stable region of less than a 10% decrease over 6000 cycles is reached with this material, which is promising. Future work should address analyzing the capacitance retention behavior of the Ag_2O-MnO_2 in detail.

We believe the long-term stability to be due to the unique hierarchical structure, particularly the lawn-like nanowire cover being stable on the spherical microparticle beneath. The nanowires of the optimal structure are relatively short, which benefits structural stability. This shortness is also beneficial because the Ag_2O increases conductivity, but it is only present in the short tips of the wires. The longer the wires are the less influence of the tips can be expected. Therefore, further improvement of this new material should aim to decrease the radius of the microsphere while leaving the nanowire cover in this dense "British lawn"-like configuration. Having less material in the spheres may not only increase the capacity per weight, but it may also abate the problematic self-activation behavior over the initial 4000 charging cycles, which may well be due to the electrolyte slowly penetrating the relatively large porous spheres. A further issue of wide interest is the role of the Ag NPs in the synthesis.

CONCLUSION

In summary, a simple and low-cost method is developed to synthesize nanowire-covered MnO_2 spheres with a superior supercapacitance of 417.2 F/g at a fast scan rate of 100 mV/s. While previously reported materials with comparable capacitances at low scan rates cannot perform well at high scan rates, the Ag_2O-MnO_2 nanowire-covered spheres have almost 80% of the low scan rate value. This makes the novel material very promising for fast charging applications and also where charging times may vary significantly while the capacitance should stay constant, as is usual for traditional applications of capacitors. Regarding long-term durability, after first passing through a temporary 50% increase of SC, the material reaches a stable region of 91.3% capacitance retention over 6000 cycles. This suggests analyzing the source of the retention behavior in future work. Apart from providing conductivity, the role of Ag is crucial in the initial and final stages of growth. The final growth mechanism involves an amorphous Ag_2O-MnO_2 mixture and has in this particular form not been reported previously. We suggested decreasing the sphere radius while keeping the dense short nanowire cover for several reasons. Better understanding and control of the initial Ag nanoparticle-dependent growth process is needed, ideally allowing for controlling it and the final stages independently of each other.

ASSOCIATED CONTENT

Supporting Information

SEM images of the prepared Ag nanoparticles, I-MnO_2, MnO_2 nanowires, products obtained via replacing Ag nanoparticles by different $AgNO_3$ concentrations, and products obtained after different reaction times. Electrochemical performances of the MnO_2 nanowires and the products with different reaction times. This material is available free of charge via the Internet at http://pubs.acs.org.

AUTHOR INFORMATION

Corresponding Author

*Tel.: +86-25-83685585. Fax: +86-25-83595535. E-mail: mengxk@nju.edu.cn.

Author Contributions

§Y. Dai and S. Tang contributed equally.

Notes

The authors declare no competing financial interest.

ACKNOWLEDGMENTS

This work was supported by the Fundamental Research Funds for the Central Universities, National Natural Science Foundation of China, State Key Program for Basic Research of China, Natural Science Foundation of Jiangsu Province, and Research Innovation Program for College Graduates of Jiangsu Province.

REFERENCES

(1) Jiang, J.; Li, Y. Y.; Liu, J. P.; Huang, X. T.; Yuan, C. Z.; Lou, X. W. Recent advances in metal oxide-based electrode architecture design for electrochemical energy storage. *Adv. Mater.* **2012**, *24*, 5166−5180.

(2) Wang, G. P.; Zhang, L.; Zhang, J. J. A review of electrode materials for electrochemical supercapacitors. *Chem. Soc. Rev.* **2012**, *41*, 797−828.

(3) Kim, T. Y.; Lee, H. W.; Stoller, M.; Dreyer, D. R.; Bielawski, C. W.; Ruoff, R. S.; Suh, K. S. High-performance supercapacitors based on poly(ionic liquid)-modified graphene electrodes. *ACS Nano* **2011**, *5*, 436−442.

(4) Yu, C. C.; Zhang, L. X.; Shi, J. L.; Zhao, J. J.; Gao, J. H.; Yan, D. S. A simple template-free strategy to synthesize nanoporous manganese and nickel oxides with narrow pore size distribution, and their electrochemical properties. *Adv. Funct. Mater.* **2008**, *18*, 1544−1554.
(5) Seredych, M.; Koscinski, M.; Sliwinska-Bartkowiak, M.; Bandosz, T. J. Charge storage accessibility factor as a parameter determining the capacitive performance of nanoporous carbon-based supercapacitors. *ACS Sustainable Chem. Eng.* **2013**, *1*, 1024−1032.
(6) Yuan, C. Z.; Yang, L.; Hou, L. R.; Shen, L. F.; Zhang, X. G.; Lou, X. W. Growth of ultrathin mesoporous Co_3O_4 nanosheet arrays on Ni foam for high-performance electrochemical capacitors. *Energy Environ. Sci.* **2012**, *5*, 7883−7887.
(7) Shaikh, J. S.; Pawar, R. C.; Moholkar, A. V.; Kim, J. H.; Patil, P. S. CuO-PAA hybrid films: Chemical synthesis and supercapacitor behavior. *Appl. Surf. Sci.* **2011**, *257*, 4389−4397.
(8) Liu, R.; Duay, J.; Lee, S. B. Redox exchange induced MnO_2 nanoparticle enrichment in poly(3,4-ethylenedioxythiophene) nanowires for electrochemical energy storage. *ACS Nano* **2010**, *4*, 4299−4307.
(9) Xia, H.; Meng, Y. S.; Yuan, G. L.; Cui, C.; Luc, L. A symmetric RuO_2/RuO_2 supercapacitor operating at 1.6 V by using a neutral aqueous electrolyte. *Electrochem. Solid-State Lett.* **2012**, *15*, A60−A63.
(10) Liu, Y. M.; Zhao, X. Y.; Li, F.; Xia, D. G. Facile synthesis of MnO/C anode materials for lithium-ion batteries. *Electrochim. Acta* **2011**, *56*, 6448−6452.
(11) Wang, X.; Li, Y. D. Selected-control hydrothermal synthesis of α- and β-MnO_2 single crystal nanowires. *J. Am. Chem. Soc.* **2002**, *124*, 2880−2881.
(12) Cross, A.; Morel, A.; Cormie, A.; Hollenkamp, T.; Donne, S. Enhanced manganese dioxide supercapacitor electrodes produced by electrodeposition. *J. Power Sources* **2011**, *196*, 7847−7853.
(13) Wang, Y. T.; Lu, A. H.; Zhang, H. L.; Li, W. C. Synthesis of nanostructured mesoporous manganese oxides with three-dimensional frameworks and their application in supercapacitors. *J. Phys. Chem. C* **2011**, *115*, 5413−5421.
(14) Li, Y.; Xie, H. Q.; Wang, J. F.; Chen, L. F. Preparation and electrochemical performances of α-MnO_2 nanorod for supercapacitor. *Mater. Lett.* **2011**, *65*, 403−405.
(15) Chen, W.; Rakhi, R. B.; Hu, L. B.; Xie, X.; Cui, Y.; Alshareef, H. N. High-performance nanostructured supercapacitors on a sponge. *Nano Lett.* **2011**, *11*, 5165−5172.
(16) Wu, Z. S.; Ren, W. C.; Wang, D. W.; Li, F.; Liu, B. L.; Cheng, H. M. High-energy MnO_2 nanowire/graphene and graphene asymmetric electrochemical capacitors. *ACS Nano* **2010**, *4*, 5835−5842.
(17) Yan, J.; Fan, Z. J.; Wei, T.; Qian, W. Z.; Zhang, M. L.; Wei, F. Fast and reversible surface redox reaction of graphene−MnO_2 composites as supercapacitor electrodes. *Carbon* **2010**, *48*, 3825−3833.
(18) Lei, Z. B.; Zhang, J. T.; Zhao, X. S. Ultrathin MnO_2 nanofibers grown on graphitic carbon spheres as high-performance asymmetric supercapacitor electrodes. *J. Mater. Chem.* **2012**, *22*, 153−160.
(19) Li, R. Z.; Ren, X.; Zhang, F.; Du, C.; Liu, J. P. Synthesis of Fe_3O_4/SnO_2 core-shell nanorod film and its application as a thin-film supercapacitor electrode. *Chem. Commun.* **2012**, *48*, 5010−5012.
(20) Bao, L. H.; Zang, J. F.; Li, X. D. Flexible Zn_2SnO_4/MnO_2 core/shell nanocable−carbon microfiber hybrid composites for high-performance supercapacitor electrodes. *Nano Lett.* **2011**, *11*, 1215−1220.
(21) Lang, X. Y.; Hirata, A.; Fujita, T.; Chen, M. W. Nanoporous metal/oxide hybrid electrodes for electrochemical supercapacitors. *Nat. Nanotechnol.* **2011**, *6*, 232−236.
(22) Wei, W. F.; Cui, X. W.; Chen, W. X.; Ivey, D. G. Manganese oxide-based materials as electrochemical supercapacitor electrodes. *Chem. Soc. Rev.* **2011**, *40*, 1697−1721.
(23) Lu, Q.; Chen, J.; Xiao, J. Q. Nanostructured electrodes for high-performance pseudocapacitors. *Angew. Chem., Int. Ed.* **2013**, *52*, 1882−1889.
(24) Wang, D. W.; Li, F.; Liu, M.; Lu, G. Q.; Cheng, H. M. 3D aperiodic hierarchical porous graphitic carbon material for high-rate electrochemical capacitive energy storage. *Angew. Chem., Int. Ed.* **2008**, *47*, 373−376.
(25) Lopez, M. C.; Ortiz, G. F.; Lavela, P.; Alcantara, R.; Tirado, J. L. Improved energy storage solution based on hybrid oxide materials. *ACS Sustainable Chem. Eng.* **2013**, *1*, 46−56.
(26) Lu, X. H.; Yu, M. H.; Wang, G. M.; Zhai, T.; Xie, S. L.; Ling, Y. C.; Tong, Y. X.; Li, Y. H-TiO_2@MnO_2//H-TiO_2@C core-shell nanowires for high performance and flexible asymmetric supercapacitors. *Adv. Mater.* **2013**, *25*, 267−272.
(27) Yang, P. H.; Xiao, X.; Li, Y. Z.; Ding, Y.; Qiang, P. F.; Tan, X. H.; Mai, W. J.; Lin, Z. Y.; Wu, W. Z.; Li, T. Q.; et al. Hydrogenated ZnO core-shell nanocables for flexible supercapacitors and self-powered systems. *ACS Nano* **2013**, *7*, 2617−2626.
(28) Toupin, M.; Brousse, T.; Belanger, D. Charge storage mechanism of MnO_2 electrode used in aqueous electrochemical capacitor. *Chem. Mater.* **2004**, *16*, 3184−3190.
(29) Tang, S. C.; Vongehr, S.; Zheng, Z.; Ren, H.; Meng, X. K. Facile and rapid synthesis of spherical porous palladium nanostructures with high catalytic activity for formic acid electro-oxidation. *Nanotechnology* **2012**, *23*.
(30) Trentler, T. J.; Hickman, K. M.; Goel, S. C.; Viano, A. M.; Gibbons, P. C.; Buhro, W. E. Solution−liquid−solid growth of crystalline III−V semiconductors: An analogy to vapor-liquid-solid growth. *Science* **1995**, *270*, 1791−1794.
(31) May, S. J.; Zheng, J. G.; Wessels, B. W.; Lauhon, L. J. Dendritic nanowire growth mediated by a self-assembled catalyst. *Adv. Mater.* **2005**, *17*, 598−602.
(32) Burke, A. Ultracapacitors: Why, how, and where is the technology. *J. Power Sources* **2000**, *91*, 37−50.
(33) Lu, X. H.; Zheng, D. Z.; Zhai, T.; Liu, Z. Q.; Huang, Y. Y.; Xie, S. L.; Tong, Y. X. Facile synthesis of large-area manganese oxide nanorod arrays as a high-performance electrochemical supercapacitor. *Energ. Environ. Sci.* **2011**, *4*, 2915−2921.